

# Stationary solutions and Neumann boundary conditions in the Sivashinsky equation

Bruno Denet

*IRPHE 49 rue Joliot Curie BP 146 Technopole de  
Chateau Gombert 13384 Marseille Cedex 13 France\**

## Abstract

New stationary solutions of the (Michelson) Sivashinsky equation of premixed flames are obtained numerically in this paper. Some of these solutions, of the bicoalescent type recently described by Guidi and Marchetti, are stable with Neumann boundary conditions. With these boundary conditions, the time evolution of the Sivashinsky equation in the presence of a moderate white noise is controlled by jumps between stationary solutions.

arXiv:physics/0604120v1 [physics.class-ph] 17 Apr 2006

---

\*Electronic address: [bruno.denet@irphe.univ-mrs.fr](mailto:bruno.denet@irphe.univ-mrs.fr)

## I. INTRODUCTION

The Sivashinsky equation [1] (or Michelson Sivashinsky equation depending on the authors) is a well established non linear equation which provides a satisfactory description of the time evolution of premixed flames. Until working on the present paper, the author had a very simple idea of the situation regarding this equation. Pole solutions of the Sivashinsky equation were obtained in [2] and popularized in [3], which reduces the time evolution of the equation to a dynamical system and the stationary solutions to finding zeroes of a non linear function of several variables. The paper [3] also shows that the poles have a tendency to coalesce, i.e. to align vertically in the complex plane. Stationary solutions were obtained in the form of coalescent solutions with a number of poles depending on the width of the domain. It was shown analytically in [4][5] that each solution, with a given number of poles is linearly stable in a given interval for the control parameter (either the domain width or more often the curvature term with a domain width fixed to  $2\pi$ ). Numerical simulations however, always performed with periodic boundary conditions, continue to show that the solutions are extremely sensitive to noise [6] for sufficiently large domains. These results are consistent with a qualitative description of the stability of curved flame fronts by Zeldovich et. al. [7].

For some reason, the author of the article began simulations of the Sivashinsky equation with Neumann boundary conditions, ie. zero slope of the flame front at each end of the domain. Of course, Neumann boundary conditions are a more realistic description of a flame in a tube than periodic boundary conditions. However, as solutions with Neumann boundary conditions on  $[0, \pi]$  are simply symmetric solutions with periodic boundary conditions on  $[0, 2\pi]$ , the author was thinking that he should obtain basically a coalescent solution, but only between 0 and  $\pi$ , with all the poles coalescing at 0, leading to a cusp at this boundary. It was so obvious that actually simulations of the Sivashinsky equation with Neumann boundary conditions were only used originally as a test case for a new computer program. However stationary solutions were obtained, where poles did not all coalesce at the same position, but actually on the two boundaries.

It turns out (although the author was absolutely unaware of this paper at the beginning of his work) that this type of stationary solutions, called bicoalescent solutions, were already discovered by Guidi and Marchetti [8]. In Section II, we show the new bicoalescent solutions

that we have obtained, which have a nice property with Neumann boundary conditions, they are stable. These solutions were not found in [8] because the curvature parameters studied were too large (or equivalently, the domain width was too small). In Section III, we show where the new solutions of Section II are found in the parameter space. We have thus to study a larger domain of the parameter space than in [8], and discover also new stationary solutions of the interpolating type described by Guidi and Marchetti (see section III for a definition of this type of solution). These interpolating solutions, unlike those of Section II, are unstable. The number of stationary solutions obtained is so large that we have entitled Section III web of stationary solutions and will try to convince the reader that this is not an exaggeration. In Section IV, the evolution of the Sivashinsky equation with noise is studied. In the case of Neumann boundary conditions, as expected, the stable bicoalescent solutions play a dominating role in the dynamics. Finally, Section V contains a conclusion.

## II. STABLE BICOALESCENT SOLUTIONS

The Sivashinsky equation can be written as

$$\phi_t + \frac{1}{2}\phi_x^2 = \nu\phi_{xx} + I(\phi) \quad (1)$$

where  $\phi(x)$  is the vertical position of the front. The Landau operator  $I(\phi)$  corresponds to a multiplication by  $|k|$  in Fourier space, where  $k$  is the wavevector, and physically to the destabilizing influence of gas expansion on the flame front (known as the Darrieus-Landau instability).  $\nu$  is the only parameter of the equation and controls the stabilizing influence of curvature. The linear dispersion relation giving the growth rate  $\sigma$  versus the wavevector is, including the two effects:

$$\sigma = |k| - \nu k^2 \quad (2)$$

As usual with Sivashinsky-type equations, the only non linear term added to the equation is  $\frac{1}{2}\phi_x^2$ . In the flame front case, this term is purely geometrical : the flame propagates in the direction of its normal, a projection on the vertical ( $y$ ) direction gives the factor  $\cos(\theta) = 1/\sqrt{1 + \phi_x^2}$ , where  $\theta$  is the angle between the normal and the vertical direction, then a development valid for small slopes of the front leads to the term  $\frac{1}{2}\phi_x^2$ . The Sivashinsky equation will be solved numerically on  $[0, 2\pi]$  with periodic boundary conditions, or (more

often in this paper) on  $[0, 2\pi]$  with only symmetric modes, which corresponds to homogeneous Neumann boundary conditions on  $[0, \pi]$  (zero slope on both ends of the domain). All dynamical calculations will be performed by Fourier pseudo-spectral methods (i.e. the non linear term is calculated in physical space and not by a convolution product in Fourier space). The method used is first order in time and semi-implicit (implicit on the linear terms of the equation, explicit on  $\frac{1}{2}\phi_x^2$ ). No particular treatment of aliasing errors has been used.

Pole solutions ([3]) of the Sivashinsky equation are solutions of the form:

$$\phi = 2\nu \sum_{n=1}^N \left\{ \ln \left( \sin \left( \frac{x - z_n(t)}{2} \right) \right) + \ln \left( \sin \left( \frac{x - z_n^*(t)}{2} \right) \right) \right\} \quad (3)$$

where  $N$  is the number of poles  $z_n(t)$  in the complex plane. Actually the poles appear in complex conjugate pairs, and the asterisk in Equation 3 denotes the complex conjugate. In all the paper, only poles with a positive imaginary part will be shown, the number of poles will also mean number of poles with a positive imaginary part. The pole decomposition transforms the solution of the Sivashinsky equation into the solution of a dynamical system for the locations of the poles. In the case of stationary solutions, the locations of the poles are obtained by solving a non linear system:

$$-\nu \sum_{l=1, l \neq n}^{2N} \cot \left( \frac{z_n - z_l}{2} \right) - i \operatorname{sgn} [\operatorname{Im} (z_n)] = 0 \quad n = 1, \dots, N \quad (4)$$

where  $\operatorname{Im} (z_n)$  denotes the imaginary part and  $\operatorname{sgn}$  is the signum function. This non linear system will be solved by a Newton-Raphson method.

Let us define here a process that will be called folding in the rest of the paper and which allows to create cellular solutions starting from curved flame fronts (i.e. fronts with only one cell in  $[0, 2\pi]$ ). If a solution  $\phi_1(x)$  of the Sivashinsky equation exists with parameter  $1/\nu_1$ , then  $\phi_2(x) = \frac{1}{m}\phi_1(mx)$  is a solution of the Sivashinsky equation with parameter  $1/\nu_2 = m(1/\nu_1)$ , with  $m$  integer.

Although we have searched for stationary solutions with periodic boundary conditions, it appears that all the solutions we have found on  $[0, 2\pi]$  are symmetric, and thus are stationary solutions with Neumann boundary conditions, i.e. zero slope, on  $[0, \pi]$ . In most of the cases the stationary solutions obtained have poles at  $x = 0$ , in a few cases however, the solutions have no poles on the boundaries (i.e. only lead to symmetric solutions with no poles at the boundary)

With periodic boundary condition, the well-known result is that in the window  $2n - 1 \leq 1/\nu \leq 2n + 1$ ,  $n = 1, 2, \dots$  there exists  $n$  different monocoalescent stationary solutions (all the poles have the same real part), with 1 to  $n$  poles, and the solution with the maximum number of poles  $n$  is asymptotically stable. For a particular value of  $1/\nu$ , the number  $n(\nu)$  such that  $2n - 1 \leq 1/\nu \leq 2n + 1$  will be called the optimal number of poles. All stable solutions found in this paper, for any value of  $1/\nu$ , even with Neumann boundary conditions, have the optimal number of poles  $n(\nu)$ .

Using however the Sivashinsky equation (Eq. 1) with Neumann boundary conditions, we obtain in each of the intervals  $[2n - 1, 2n + 1]$  of the parameter  $1/\nu$ , not only one asymptotically stable solution, but several, of the form  $(l, n - l)$  with  $l = 0, 1, \dots, n$  where  $l$  poles coalesce at  $x = 0$  and  $l - n$  coalesce at  $x = \pi$  (The bicoalescent type of solutions have been recently introduced in [8]). These solutions will also be obtained from the non linear system of equations (Eq. 4) in Section III. It must be remarked that all these solutions, except the monocoalescent one, are unstable for periodic boundary conditions, i.e. when antisymmetric perturbations are allowed on  $[0, 2\pi]$ . We have just defined here the notation  $(n_1, n_2)$  that will be used in the paper for bicoalescent solutions with  $n_1$  poles at zero, and  $n_2$  at  $\pi$ . Monocoalescent solutions can be seen as a particular case of bicoalescent solutions and will be noted  $(n, 0)$ . We will encounter also multicoalescent solutions, such as  $(n_1, n_2, n_3, \dots)$ , which means that in the interval  $[0, 2\pi]$ , the poles coalesce at different locations:  $n_1$  poles coalesce at a position on the left of the interval, generally 0,  $n_2$  poles coalesce at a position with a higher value of  $x$ , then  $n_3$  at a position with a value of  $x$  even higher, and so on. With this notation  $(1,1,1)$  represents a cellular solution with three cells obtained by the folding of the  $(1,0)$  solution.

For the particular value  $1/\nu = 10.5$  (five poles) the different possible solutions are shown on  $[0, \pi]$  in Figure 1. On the left, we have a monocoalescent  $(5,0)$  solution with five poles at 0. The middle solution of the figure is a  $(4,1)$  solution (4 poles at  $x = 0$ , 1 pole at  $x = \pi$ ). Finally the solution on the right is a  $(3,2)$  solution (3 poles at 0, 2 poles at  $\pi$ ). For an even value of the optimal number of poles (i.e. the value of  $n$  in the interval  $[2n - 1, 2n + 1]$ ), the stable solutions will include a solution symmetric on  $[0, \pi]$ , for instance if  $n = 6$  we have the solutions  $(6,0)$   $(5,1)$   $(4,2)$  and the symmetric  $(3,3)$  solution. In Figure 2, we show on the same figure the shape  $(x, \phi(x))$  ( $x$  is the horizontal direction) of the  $(3,2)$  solution for  $1/\nu = 10.5$  with  $x \in [0, \pi]$  (lower part of the figure, below the horizontal segment) and the

corresponding locations of poles in the complex plane (upper part of the figure, above the horizontal segment). The poles are indicated by circles, the segment is the real axis in pole space between 0 and  $2\pi$ . The important thing about this type of figure, which will be used in the rest of the paper, is that a pole very close to the real axis (i.e. very close to the horizontal segment in the upper part of the figure) leads to a cusp in the front shape (in the lower part of the figure), and that the  $x$  value of the pole in the complex plane is the same as the  $x$  value in physical space of the cusp that appears; in a diagram like Figure 2, the cusp and the corresponding pole are on the same vertical line. We will see later however examples of poles far away from the real axis with no cusp at the  $x$  value of the pole. This effect results from a competition between a new pole and the poles at zero which tend to prevent the appearance of a new cusp. It is described in a simple way in Appendix A.

An illustration of the stability of the (3,2) stationary solution is given in Figure 3. The initial condition used in the Sivashinsky equation, with Neumann boundary conditions, is exactly the (3,2) solution for  $1/\nu = 10.5$ . In a simulation without noise, the amplitude (maximum minus minimum of  $\phi(x)$ ), would simply stay constant with time, as the (3,2) solution is stable. In order to complicate the convergence to the (3,2) solution, we apply a noise (additive gaussian white noise added to the Sivashinsky equation, amplitude  $a = 0.01$ , see section IV for other examples of simulation with noise, and other explanations) when time  $< 10$ , and then continue the simulation without noise up to a time of 500. The stability of the (3,2) stationary solution for Neumann boundary conditions is illustrated by the fact that the shape returns quickly to this solution (observe the fact that the final amplitude is exactly the same as the initial one).

Of the different stable stationary solutions just described, the largest basin of attraction (with initial conditions close to a flat flame with some random perturbations) corresponds to the most symmetric solution (i.e. the (3,2) solution for 5 poles) and the monocoalescent solution ((5,0) in the previous case). It even seems, if one compares both types of solutions, that the most symmetric solution has a larger basin of attraction for low values of  $1/\nu$  (in the case of five poles for instance), and the monocoalescent one a larger basin for large  $1/\nu$ . However, this result could be limited to this type of initial conditions. Actually, in Section IV, it will be shown that in the presence of a moderate white noise added to the Sivashinsky equation, the solution is much more often close to the most symmetric bicoalescent solution with the optimal number of poles than close to the corresponding monocoalescent solution.

Before closing this section, let us note the analogy of the bicoalescent solutions found here with cellular solutions observed experimentally in directional solidification [9]. These solutions, called doublets, look almost the same as the bicoalescent solutions of this section. They are also stable for some range of parameters. However, a major difference is that there is no instability at large scale in directional solidification, and that as a result, the structure with one small cusp, one large cusp can be repeated a number of times in the overall doublet cellular structure. But in both cases, flames (bicoalescent solutions) and directional solidification (doublets), these type of stationary solutions are related to the well-known phenomenon of tip-splitting of curved fronts [10].

### III. WEB OF STATIONARY SOLUTIONS

As most of the solutions of the previous section were not found by Guidi and Marchetti, only some trivial, cellular solutions obtained by folding, such as the (2,2) solution, we investigate in this section higher values of  $1/\nu$  than those used in their paper [8]. As in this paper, we plot the stationary solutions in a diagram giving the amplitude (maximum minus minimum value of the solution) versus  $1/\nu$ .

A light version of this diagram, with only the most important solutions, particularly the bicoalescent solutions of the previous section, is shown in Figure 4. The complete version of this diagram, with all the solutions obtained by the author, will be shown in Figure 5. We have found it necessary to use two figures, because the different solutions are so close in Figure 5 that it is difficult at first sight to recognize a particular bicoalescent solution in this figure. We hope that a comparison between Figures 4 and 5 can help the reader understand how the bicoalescent solutions of the previous section are interconnected to the rest of the stationary solutions, particularly the cellular ones. But the author knows, it is not an easy task for the reader, so for the moment, we only start with the simplified version of the diagram. To be more precise, we plot in Figure 4 the basic solutions, i.e. the solutions with  $n$  poles whose branch exists in the interval  $[2n - 1, 2n + 1]$  of the parameter  $1/\nu$ . In this interval, these type of solutions have thus the optimal number of poles, a necessary condition for the solution to be stable, as explained in Section II.

In dashed lines in Figure 4 can be seen the monocoalescent solutions  $(n, 0)$  which are created at  $1/\nu = 2n - 1$  and are stable in the periodic case until the next solution  $(n + 1, 0)$

is created. From these solutions, by a process we call here folding and which is defined in the previous section, the solutions (1,1) (1,1,1) ... (dotted lines) are created, as well as the bicoalescent (1,1) (2,2) (3,3) ... The non trivial bicoalescent solutions of Section II are created starting from these symmetric bicoalescent solutions. The hierarchy (2,1) (3,1) (4,1) (5,1)... is created starting from the (1,1) solution obtained by folding. The hierarchy (3,2) (4,2) ... emerges from the (2,2) solution. Finally, In Figure 4 the solution (4,3) (first element of the hierarchy (5,3) (6,3) ...) is created from the (3,3) solution, which means that one pole comes from infinity at a given value of  $1/\nu$  to create the solution.

All the solutions of the previous hierarchies are plotted as solid black lines in Figure 4. With the exception of the folded symmetric solutions, all the other bicoalescent solutions of this figure are stable when they are created, until a new solution with one more pole appears. This behavior is exactly similar to the monocoalescent solutions, the intervals of stability are also the same.

In solid gray lines in Figure 4 are plotted however another hierarchy of solutions. This hierarchy contains solutions of the type (2,1,1) (3,1,1) (4,1,1) apparently created exactly on the same intervals as before. Of course this hierarchy only leads to unstable solutions, in the periodic as well as the Neumann case. It seems reasonable to suggest that as  $1/\nu$  increases, an infinite number of hierarchies will be created, each starting from a suitable folded solution. The author actually suggests the following conjecture: for each value  $1/\nu$  of the control parameter with optimal number of poles  $n(\nu)$ , all the multicoalescent stationary solutions having the optimal number of poles, labelled  $(n_1, \dots, n_p)$  for any  $p$  in the interval  $1 \leq p \leq n(\nu)$ , with  $\sum_{i=1}^p n_i = n(\nu)$ , do exist.

Furthermore, as the amplitude of the solutions in these hierarchies increases with  $1/\nu$ , it is extremely likely that solutions of the  $(n, 1)$  hierarchy for instance, will soon become extremely close to the corresponding monocoalescent solution  $(n+1, 0)$ . And in the Neumann case, all the bicoalescent hierarchies lead to stable stationary solutions. A study of the time evolution of solutions of the Sivashinsky equation will be reported in Section IV.

The previous argument suggests that there are many stationary solutions of the Sivashinsky equation. However, as seen in Figure 5, Figure 4 was a very simplified version of the diagram, with only the most important stationary solutions, which were called basic solutions (see the explanation above), and form a sort of skeleton of the entire structure of the solutions. We have called this structure web of stationary solutions for obvious reasons, all

the solutions are interconnected, even the number of jumps necessary to go from one solution to one another can probably be defined, reminiscent of the hops from router to router on the internet. It is to be noted that the other well-known Sivashinsky-type equation, the Kuramoto-Sivashinsky equation, also admits a huge number of stationary solutions [11]. The author does not even claim to have obtained in Figure 5 something comprehensive in the parameter space studied. The reader is again warned that it is easier to look at both figures 4 and 5 at the same time, to locate first the basic solutions that a particular interpolating solution connects.

The new solutions compared to Figure 4 are of the interpolating type discussed by Guidi and Marchetti. We define here these interpolating solutions (as opposed to basic solutions) as solutions whose branch does not exist in the interval  $[2n - 1, 2n + 1]$  of the parameter  $1/\nu$ . Thus these solutions do not have the optimal number of poles and cannot be stable (starting from such a solution, a pole would come from infinity or disappear at infinity and a solution with the optimal number of poles would be created). But in Figure 5, it can be seen that these interpolating solutions typically connect different basic solutions of the previous bifurcation diagram (Figure 4).

For instance, if one starts from the cellular solutions  $(1,1,1,\dots)$ , there exists interpolating solutions starting from this solution and leading to all cellular solutions and the mono-coalescent solutions above. It must be noted that the precise values of  $1/\nu$ , where these interpolating branches appear from the cellular solutions, were calculated analytically in [12]. In the simple case of the  $(1,1,1)$  solution already studied by Guidi and Marchetti, it is possible to move the poles vertically in the complex plane in two different ways in order to have an initial guess of the position of the poles on the interpolating branches (the Newton iteration leading to the true values of the positions of the poles). Each interpolating solution emanating from a cellular solution can be labelled by the way the poles move along the interpolating branch compared to the cellular solution. This type of pole movement along the interpolating branch (at the beginning, where the branch is created) corresponds exactly to the way the poles of the cellular solutions must be moved in order to obtain an initial guess that will converge. So we have the  $(+,-,+)$  solution: two poles are moved upward in the complex plane (i.e. their imaginary part increases, while the real part is kept constant), one downward compared to the  $(1,1,1)$  solution. This  $(+,-,+)$  solution will interpolate, starting from the three cells solution, all the monocoalescent solutions  $(1,0)$   $(2,0)$  and  $(3,0)$  (this part

of the diagram will be described in more details later). We have also the  $(-,+,-)$  solution, which, as seen in the figure, interpolates the  $(1,1)$  solution (one pole going at infinity at this point).

If we look at a much more complicated case, the five poles  $(1,1,1,1,1)$  solution, it seems that in order to get the interpolating solutions, we have to consider at least three levels of vertical movement of the imaginary part of the poles, and for instance one interpolating solution has been constructed by moving the third pole upward, the first and fifth downward, the second and fourth somewhere in between. Unfortunately, as shown in the case of the interpolating solutions emanating from the six poles cellular  $(1,1,1,1,1,1)$  solution, the author's capacities have been exceeded and neither the solution interpolating  $(1,0)$   $(2,0)$   $(3,0)$   $(4,0)$   $(5,0)$   $(6,0)$ , neither the one interpolating  $(1,1,1,1)$  have been found. Actually, although it is more or less obvious that these solutions exist, the present author has been unable to generate initial pole locations converging to these solutions (which probably means that the author has not understood what type of perturbation of the cellular solution leads to these two branches).

If the way the monocoalescent solutions are interpolated starting from the cellular solutions is now considered, we prefer to start now from the monocoalescent solution, for instance the  $(6,0)$  solution, and decrease  $1/\nu$ . In Figure 4, the monocoalescent solutions were appearing suddenly apparently from nothing, for some value of the control parameter. On the contrary, in Figure 5, precursors of the monocoalescent solution exist. So if the  $(6,0)$  solution appears at  $1/\nu = 11$ , what do we have exactly before ?

Actually, between  $1/\nu = 11$  and  $1/\nu = 10$ , the precursor of  $(6,0)$  is a bicoalescent  $(5,1)$  solution, with five poles at zero, one at  $\pi$ , however, the last one is very far from the real axis, and does not lead to a cusp in the solution. This type of bicoalescent solution, apart from the folded solutions like  $(2,2)$ , were the only ones obtained in Guidi and Marchetti (they have obtained actually the  $(3,1)$  solution interpolating  $(4,0)$  and the  $(2,1)$  interpolating  $(3,0)$ ). They are unstable even for Neumann boundary conditions, because they do not have the optimal number of poles corresponding to the control parameter (the optimal number was defined in Section II).

Between  $1/\nu = 10$  and  $1/\nu = 9$ , the solution is no more bicoalescent, but is instead a  $(4,1,1)$  solution. Then on  $[8, 9]$  we have a  $(3,1,1,1)$  solution, on  $[7, 8]$  a  $(2,1,1,1,1)$  solution, and as said before, we have not obtained the precursor close to the six poles cellular solution.

It is also possible to explain the previous claim that the precursors of (6,0) interpolate all the monocoalescent solutions with a number of poles less than 6. At  $1/\nu = 11$ , one of the six poles at zero goes to infinity, and reappears at  $\pi$  to give a (5,1) solution. At  $1/\nu = 10$ , the pole at  $\pi$  and one of the poles at zero go to infinity, and reappear later to give a (4,1,1) solution, and so on. The fascinating point is that although all the precursors appear different, the curve of the amplitude of all the precursors and of the final monocoalescent solution versus the control parameter looks perfectly smooth. This, as well as the overall structure of Figure 5, suggests that symmetries less obvious than those leading to the folded solutions could be at work in the Sivashinsky equation.

Let us look now at the shape of all these precursors in physical space. We consider as before the case  $\nu = 10.5$  (optimal number of poles : 5) . We show in Figure 6 different curved flame solutions. The one with the higher amplitude is the stable monocoalescent (5,0) solution. Then we have, with smaller amplitude, a six poles (5,1) solution interpolating (6,0). Then we have the four poles (4,0) solution, a seven poles (4,1,1,1) solution interpolating (7,0), the three poles (3,0) solution, and an eight poles (3,1,1,1,1,1) interpolating (8,0). We have stopped there, as the next solutions in this list have an amplitude very different from the original (5,0). The interesting point is that in Figure 6, all these solutions, which have a very different number of poles, look relatively similar, like subsided versions the original monocoalescent solution, the first ones being very close to (5,0) (and will be even closer with increasing  $1/\nu$ ). It seems that this is the way the Sivashinsky equation is recovering a continuum of curved flame solutions in the limit  $1/\nu \rightarrow \infty$ , something like the continuum of Ivantsov parabola of the related solidification problem [10]. From the simulations of Section IV, it is not obvious at all that these subsided unstable stationary solutions close to the monocoalescent play any particular role in the dynamics, except perhaps by providing ways to escape the stable monocoalescent solution during the transient phase. We have shown in the successive Figures 7, 8 and 9 the solutions and their poles for the non trivial cases (5,1), (4,1,1,1) and (3,1,1,1,1,1) respectively. Once again, it highlights the fact that the presence of poles is not equivalent to the presence of cusps, sufficiently far from the real axis, and with other poles much closer, some poles only lead to solutions with a weaker amplitude (see Appendix A).

Now, if we take another look at the stable bicoalescent solutions of Section II, the same phenomenon as for monocoalescent solutions has to be observed: the bicoalescent solutions

do not appear from nothing at a precise value of the parameters, they have precursors, as seen in Figure 5. For instance, we have produced precursors of the  $(n, 1)$  hierarchy, which also look like subsided versions of the corresponding stable bicoalescent solutions, and will also be closer to the original solution as  $1/\nu$  increases.

Overall, the bifurcation diagram going from cellular to curved flame fronts with all the interpolating solutions of Figure 5 has a structure totally unexpected. In the Sivashinsky equation case, most of the cellular solutions are unstable. However, the addition of a sufficient amount of gravity (flames propagating downward) to the Sivashinsky equation is known to stabilize these solutions and to create a complex transition from cellular to curved fronts when gravity is varied [13][14]. It remains to be seen if the structure of this transition has any relation with Figure 5, which is likely, as a stable stationary solution close to the bicoalescent solutions of the present paper was found in [14]. But searching for stationary solution with gravity is much more difficult than with the Sivashinsky equation, as no pole decomposition exists. The author takes this opportunity to say that the instabilities of curved flames observed with a very small gravity (and with periodic boundary conditions) in [15] would probably disappear with Neumann boundary conditions, as the most violent instabilities of this paper are created by antisymmetric modes.

#### IV. EVOLUTION WITH NOISE

In Figure 10, we start by showing a typical time evolution with periodic boundary conditions, and a white noise added to the right hand side of the Sivashinsky equation. This white noise is gaussian, with zero mean value and deviation one, and we multiply it by an amplitude  $a$ .  $a = 0.01$  and  $1/\nu = 11.5$  (optimal number of poles: six) in the simulations presented in this section, with periodic and Neumann boundary conditions. In Figure 10 is plotted, for periodic boundary conditions, the amplitude of the front versus time, the initial condition being a five poles solution which is not stationary for this value of the control parameter, and leads to the initial transient.

After this transient, the solution oscillates violently between low and high values of the amplitude. The peak values correspond to curved front solutions, with the poles being apparently almost monocoalescent, but with an amplitude much higher than the monocoalescent  $(6,0)$  stationary solution. The values of the amplitudes for the stationary solutions

(6,0) (5,1) (4,2) (3,3) are all indicated in the figure by gray lines, so that the reader can compare. The low values correspond to shapes with a new cusp formed in the flat part of the front. For the lowest values of the amplitude, this new cusp leads almost to a bicoalescent solution, but with again an amplitude which seems higher than the (5,1) or (4,2) stationary solution. The solution never comes close to the (3,3) solution, which on  $[0, 2\pi]$  is a two cells solution. Furthermore, other low values of the amplitude correspond to a cusp that develops without being exactly centered. Anyway, the dynamics is dominated in the periodic case by antisymmetric perturbations. Even if the new cusp formed by the perturbation is correctly centered when it forms, it will ultimately move on one side, and will be swallowed by the main cusp. This of course modifies the position of the main cusp, and leads to the very high peak amplitudes observed. This antisymmetric dynamics is forbidden for Neumann boundary conditions, so let us see now what happens in this case.

The situation is shown in Figure 11, for the same control parameter and noise amplitude as in the periodic case. Before discussing this figure in detail, the overall impression is that the signal obtained is much less turbulent. The different stationary solutions for this value of the control parameter are also indicated by gray lines.

The first point to note is that in this figure, except in the initial transient, the front is never monocoalescent. Even for the peak values obtained, where the amplitudes obtained sometimes seem close to the (6,0) amplitude, we stress that all the solutions obtained at the peak value are bicoalescent and not monocoalescent. On the contrary, the solution seems often close to the different bicoalescent (3,3) (4,2) and (5,1) solutions. We show in Figure 12 a comparison between the solution at time 410.555 in Figure 11 (dashed dotted line), where the amplitude has a local minimum very close to the amplitude of the (4,2) solution, and the shape of the (4,2) solution for  $1/\nu = 11.5$  (solid line). The agreement between both solutions is excellent in this case. For very small values of the noise amplitude (not shown here) the solution (with Neumann boundary conditions) actually oscillates around the (3,3) solution, without making jumps to any of the other stable stationary solutions. As the noise used here is gaussian, it is not impossible however, that jumps could occur as extremely rare events (for very small noise amplitudes), and could be observed in very long simulations.

The value of the noise taken here  $a = 0.01$ , although moderate, is already sufficient to produce jumps in the amplitude, often actually jumps between the bicoalescent steady solutions. The very low values of the amplitude in Figure 11 correspond to shapes with three

cusps in  $[0, \pi]$ , one on each boundary, and one in the middle. For this value of the control parameter, the middle cusp is always smaller than the cusps on the side. It is the author's opinion that the lowest values of the amplitude correspond to a shape close to an unstable stationary solution, which has not been found in Figure 5. As the solution does not need to be symmetric on  $[0, \pi]$ , the mechanism for the disappearance of the middle cusp is relatively similar to the same one on  $[0, 2\pi]$  in the periodic case, the middle cusp moves on one side and is swallowed by one of the two main cusps. The difference here with the periodic case is that the main cusp does not move after having swallowed the small cusp and stays on the boundary.

After the low values of the amplitude comes a transient, where the amplitude very quickly grows towards a peak value, which is a very unstationary bicoalescent solution. Depending on the noise, the shape will then often come back close to a stationary bicoalescent solution. Finally, it seems that higher noise amplitudes or larger  $1/\nu$  (the type of signal obtained is very sensitive to this last value) lead to more turbulent curves of amplitude versus time with more jumps and more time spent in the unstable low amplitudes solutions and the very unstationary peaks.

To conclude this section, let us compare the behavior with Neumann and periodic boundary conditions. For small  $\nu$ , the stable stationary solutions are very sensitive to external noise in both cases. As is well-known in the periodic case (and in this respect, the situation is very similar with Neumann boundary conditions), small perturbations are continuously created on the front. But the difference lies in the symmetries. In the periodic case, the stable stationary solutions are the monocoalescent solution with the optimal number of poles, and the continuum of its lateral translations, all neutrally stable because of this symmetry. The noise keeps disturbing the monocoalescent solution, but another solution of the continuum of monocoalescent solutions (with the optimal number of poles) is also continuously recreated. With Neumann boundary conditions, the stable solutions are now the bicoalescent solutions with the optimal number of poles. The perturbations created by the noise now serve to explore the different stable bicoalescent solutions, causing jumps between two different bicoalescent solutions. But with Neumann boundary conditions, all stable solutions are not created equal, some are easier to destabilize than the others. As seen previously for instance, the monocoalescent solution is more sensitive to noise. As a result, during the time evolution, the front will almost never be close to the monocoalescent solution for small

$\nu$  (which is just the opposite of the behavior with periodic boundary conditions).

## V. CONCLUSION

To summarize this paper, new bicoalescent solutions of the Sivashinsky equation, stable in the Neumann case, have been obtained. They have found their location in the incredible structure of the web of stationary solutions. Simulations for moderate noise show that the evolution is controlled by jumps between stationary solutions. The author would like to insist here on the most important point of this paper: evolution with periodic (controlled by antisymmetric perturbations) and Neumann boundary conditions is very different. The Neumann boundary conditions are more realistic, although in the presence of heat losses, the flame is no more perpendicular to the wall (and is of course three dimensional). Finally, it is likely that new analytical studies of the Sivashinsky equation should be possible: even if the equation is now almost thirty years old, many things remain to be explained.

### Appendix A: HOW FAR MUST A POLE BE LOCATED FROM THE REAL AXIS TO CREATE A NEW CUSP?

In this appendix, we will try to explain in a very simplified way that adding a new pole to a monocoalescent solution does not necessarily create a new cusp if the isolated pole is located too far from the real axis. Let us consider the following idealized situation: we have a monocoalescent stationary solution with poles located at 0. A new pole at  $\pi$  is added to this solution, without moving any of the other poles coalesced at 0. The front with the new pole is no more stationary, but in this appendix, we try to answer the following question: at which distance of the new pole to the real axis is a new cusp created? We call this distance  $y_c$  and its value will be measured numerically for different values of  $1/\nu$ , with an optimal number of poles. In real situations the presence of the pole at  $\pi$  modifies the position of the poles at 0, particularly the poles located far from the real axis. We neglect this effect as we just want to have a reasonable order of magnitude of the value of  $y_c$  leading to a new cusp.

It turns out that the value of  $y_c$  can be computed analytically in the continuous approximation introduced by Thual Frisch and Hénon [3]. Instead of summing on every pole located at 0, this discrete sum is replaced by an integral, with a pole density  $\rho(y)$  ( $y$  being

the vertical coordinate in the complex plane) given by (see [3] for a derivation):

$$\rho(y) = \frac{1}{\pi^2\nu} \ln \left( \coth \frac{|y|}{4} \right)$$

The value of the slope of the front  $\phi_x$  corresponding to the coalesced poles at 0 (in the continuous approximation) and to the isolated pole at  $\pi$  is given by:

$$\phi_x(x) = -\nu P \int \rho(y) \cot \left( \frac{x-iy}{2} \right) dy - \nu \cot \left( \frac{x-\pi-iy_1}{2} \right) - \nu \cot \left( \frac{x-\pi+iy_1}{2} \right)$$

where  $P$  denotes the principal value of an integral going from  $-\infty$  to  $+\infty$ , the conjugated isolated poles being located at  $\pi \pm iy_1$ . As a criterion for the appearance of a new cusp, we choose the natural condition  $\phi_{xx}(x = \pi) < 0$ . The value of  $\phi_{xx}$  at this point is created by the competition between the coalesced poles at 0, which tend to prevent the creation of the new cusp, and the isolated pole (and its complex conjugate) which has the opposite effect. With the previous forms of the slope and the pole density, we obtain:

$$\phi_{xx}(x = \pi) = P \int \frac{1}{2\pi^2} \ln \left( \coth \left( \frac{|y|}{4} \right) \right) \frac{1}{\cosh^2(y/2)} dy - \frac{\nu}{\sinh^2(y_1/2)}$$

Integrating by parts, the antiderivative of the function under the integral sign is

$$\frac{1}{\pi^2} \left( \ln \left( \coth \left( \frac{|u|}{2} \right) \right) \tanh(u) + 2 \arctan(\exp(u)) \right)$$

with  $u = y/2$ , leading finally to

$$\phi_{xx}(x = \pi) = \frac{1}{\pi} - \frac{\nu}{\sinh^2(y_1/2)}$$

In this formula, the term  $1/\pi$  comes from the poles at 0, the other term from the isolated pole at  $\pi$ . As said before, these two terms have different signs. The condition  $\phi_{xx}(x = \pi) = 0$  finally leads to the value of  $y_1 = y_c$  corresponding to the appearance of a cusp, which is:

$$y_c = 2 \operatorname{arcsinh}(\sqrt{\pi\nu})$$

The cusp only appears if  $y_1 < y_c$ . We now compare in Figure 13 this formula to the values of  $y_c$  measured numerically for  $1/\nu = 10$  (5 poles at 0, one at  $\pi$ ), 20 (10+1 poles), 40, 60, 80, 100 (50+1 poles), each time with the optimal number of poles coalesced at 0 and one extra pole at  $\pi$ . The solid curve is the previous formula obtained in the continuous approximation, the circles are the values measured numerically. It can be seen that the

agreement is good. It is even more surprising if we think that for  $1/\nu = 10$  we have only five poles at 0 and the continuous approximation for the second order derivative at  $\pi$  works correctly, the numerical point is just slightly below the theoretical curve. Of course, this result is obtained in the framework of an illustrative model where all the positions of the poles are kept fixed, but it serves to justify the fact that in the presence of other poles, a new pole at a different  $x$  coordinate needs to be sufficiently close to the real axis to create a new cusp.

- 
- [1] G. Sivashinsky, *Acta Astronautica* **4**, 1117 (1977).
  - [2] Y. Lee and H. Chen, *Phys. Scr.* **2**, 41 (1982).
  - [3] O. Thual, U. Frisch, and M. Hénon, *J. Phys. France* **46**, 1485 (1985).
  - [4] D. Vaynblatt and M. Matalon, *Siam J. Appl. Math.* **60**, 679 (2000).
  - [5] D. Vaynblatt and M. Matalon, *Siam J. Appl. Math.* **60**, 703 (2000).
  - [6] Z. Olami, B. Galanti, O. Kupervasser, and I. Procaccia, *Phys. Rev. E* **55**, 2649 (1997).
  - [7] Y. Zeldovich, A. Istratov, N. Kidin, and V. Librovich, *Combust. Sci. Tech.* **24**, 1 (1980).
  - [8] L. Guidi and D. Marchetti, *Physics Letters A* **308**, 162 (2003).
  - [9] H. Jamgotchian, R. Trivedi, and B. Billia, *Phys. Rev. E* **47**, 4313 (1993).
  - [10] P. Pelcé, *Dynamics of curved fronts* (Academic Press, Boston, 1988).
  - [11] J. Greene and J. Kim, *Physica D*. **33**, 99 (1988).
  - [12] M. Renardy, *Physica D* **28D**, 155 (1987).
  - [13] B. Denet, *Combust. Sci. Tech.* **92**, 123 (1993).
  - [14] B. Denet and J. Bonino, *Combust. Sci. Tech.* **99**, 235 (1994).
  - [15] B. Denet, *Europhys. Lett.* **21**, 299 (1993).

Figure 1: Flame shapes  $(x, \phi(x))$  with  $x \in [0, \pi]$  of the (from left to right) (5,0) (4,1) and (3,2) stationary solutions for  $1/\nu = 10.5$ . All scales are the same in the  $x$  and  $y$  direction

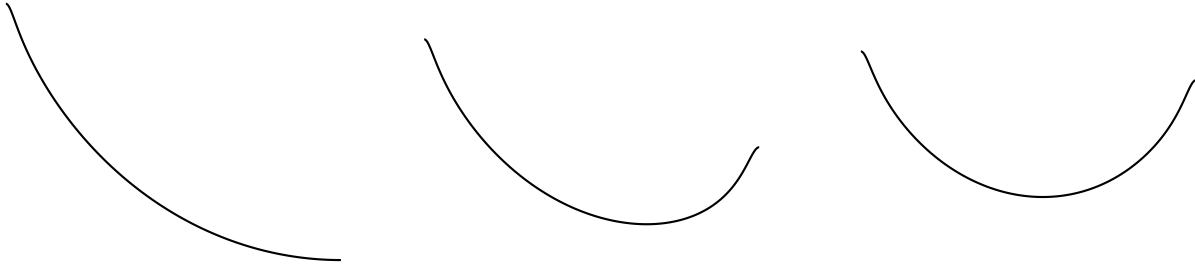


Figure 2: Lower part of the figure (below the horizontal segment) : flame shape  $(x, \phi(x))$  with  $x \in [0, \pi]$  of the (3,2) stationary solution for  $1/\nu = 10.5$ . Upper part of the figure (above the horizontal segment) : corresponding pole locations in the complex plane (the segment is the real axis in the complex plane between 0 and  $2\pi$ , the poles are indicated by circles). All scales are the same in the  $x$  and  $y$  direction, both for the flame shape and for the poles.

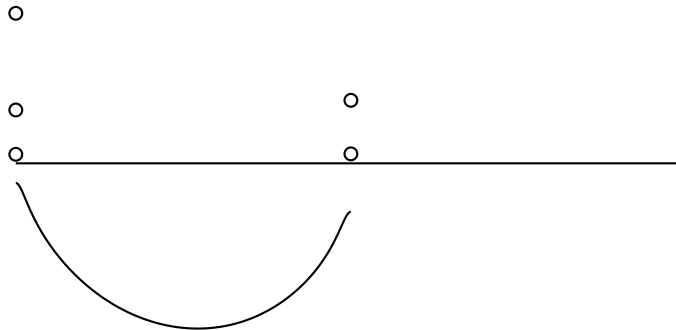


Figure 3: Amplitude versus time with Neumann boundary conditions for  $1/\nu = 10.5$ . The initial condition is the (3,2) stationary solution. A gaussian white noise (amplitude  $a = 0.01$ ) is imposed on this solution when time  $< 10$ , and is then suddenly stopped. The solution goes back to the (3,2) solution for large times.

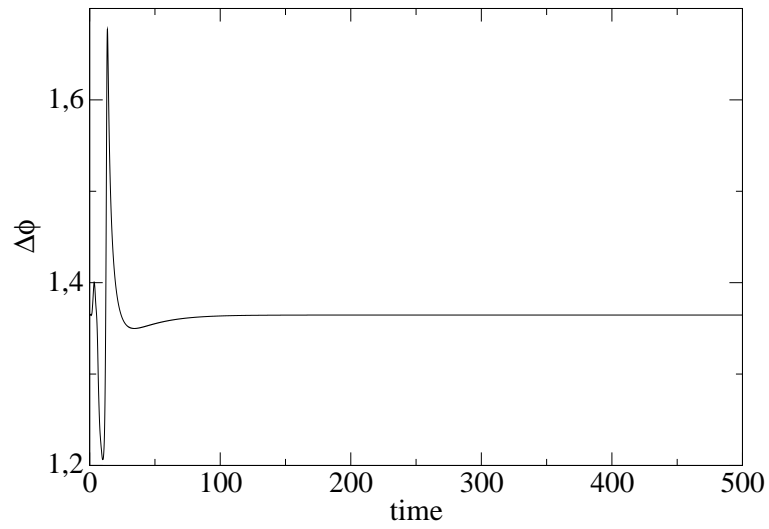


Figure 4: Stationary solutions: amplitude  $\Delta\phi$  versus  $1/\nu$  (light version with the monocoalescent solutions  $(n,0)$ , the cellular solutions  $(1,1,1,\dots)$ , and the stable bicoalescent solutions  $(p,q)$ )

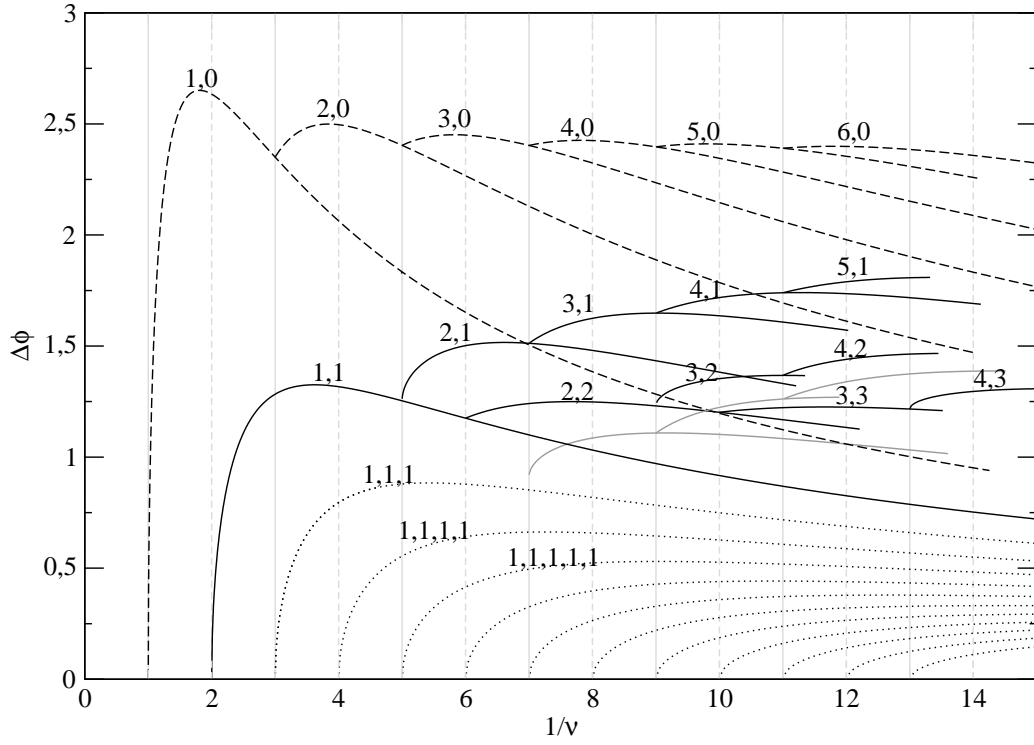


Figure 5: Stationary solutions: amplitude  $\Delta\phi$  versus  $1/\nu$  (complete version of the solutions obtained by the author, including the interpolating solutions).

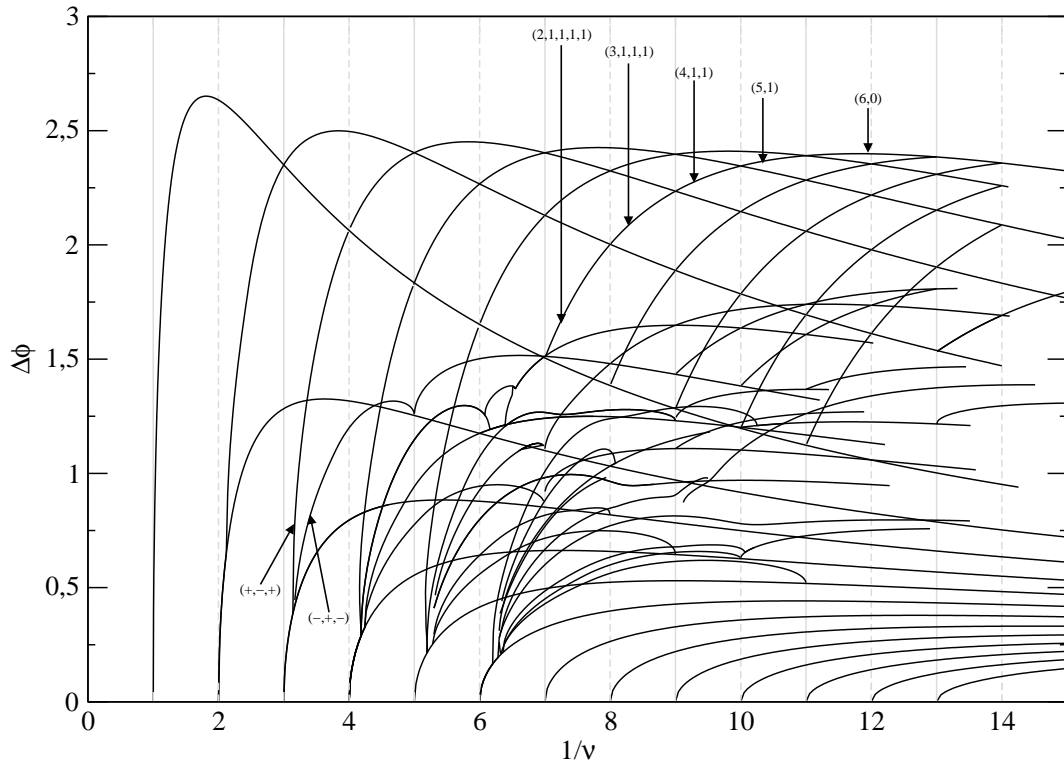


Figure 6: Different curved front solutions ( $\phi(x)$ ) with  $x \in [0, \pi]$  for  $1/\nu = 10.5$ . A constant has been added to each solution in order to have the same spatial mean value for all the solutions presented in this figure.

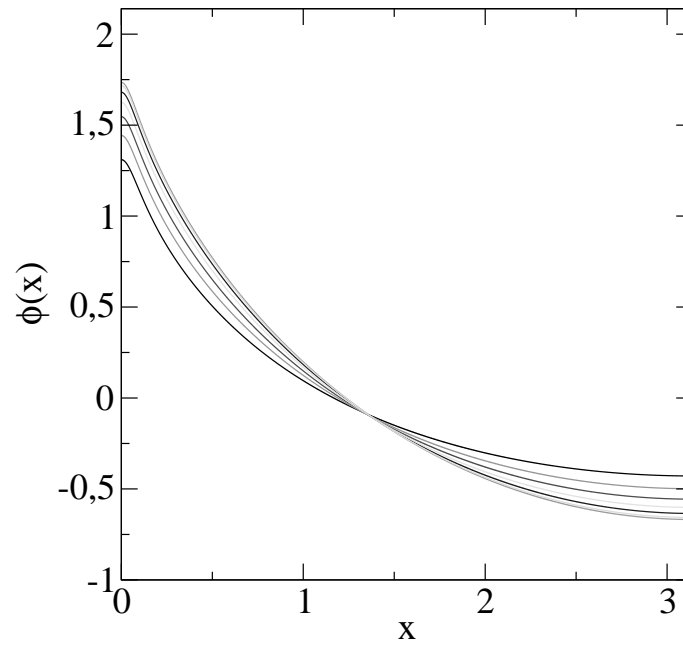


Figure 7: Interpolating (5,1) solution for  $1/\nu = 10.5$ : lower part of the figure, flame shape, upper part of the figure: pole locations (see Fig. 2 for a more complete description of this kind of figure)

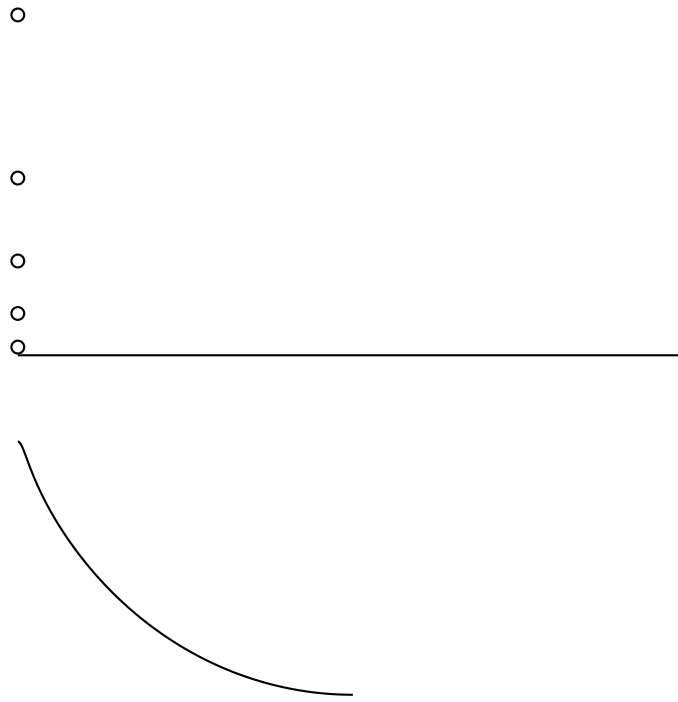


Figure 8: Interpolating  $(4,1,1,1)$  solution for  $1/\nu = 10.5$ ; lower part of the figure, flame shape, upper part of the figure: pole locations (see Fig. 2 for a more complete description of this kind of figure)

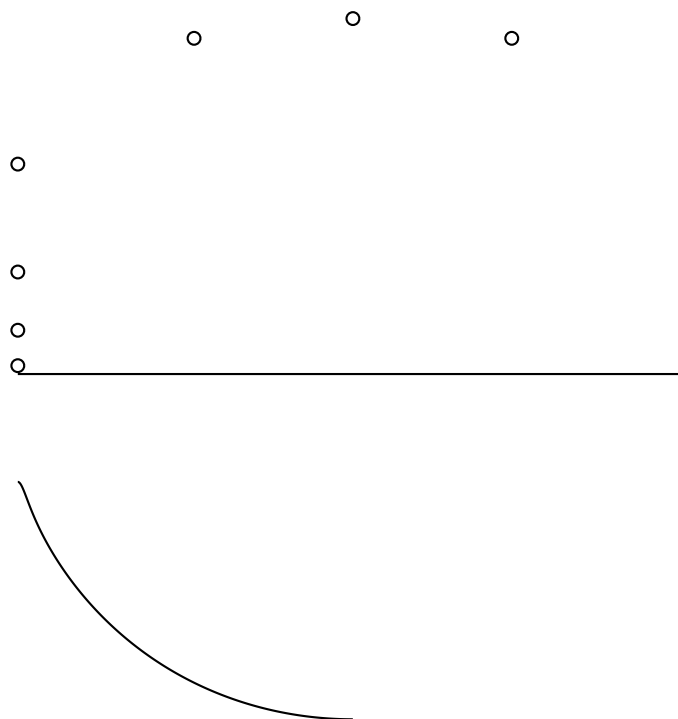


Figure 9: Interpolating  $(3,1,1,1,1)$  solution for  $1/\nu = 10.5$ : lower part of the figure, flame shape, upper part of the figure: pole locations (see Fig. 2 for a more complete description of this kind of figure)

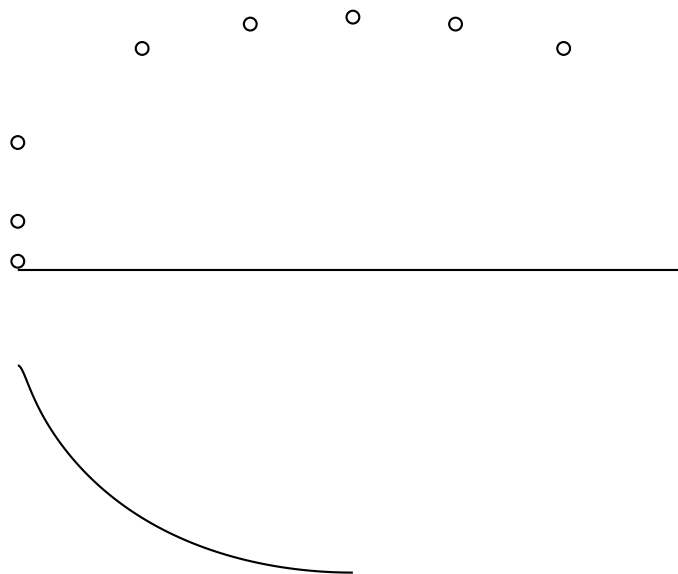


Figure 10: Amplitude versus time with periodic boundary conditions for  $1/\nu = 11.5$  and  $a = 0.01$

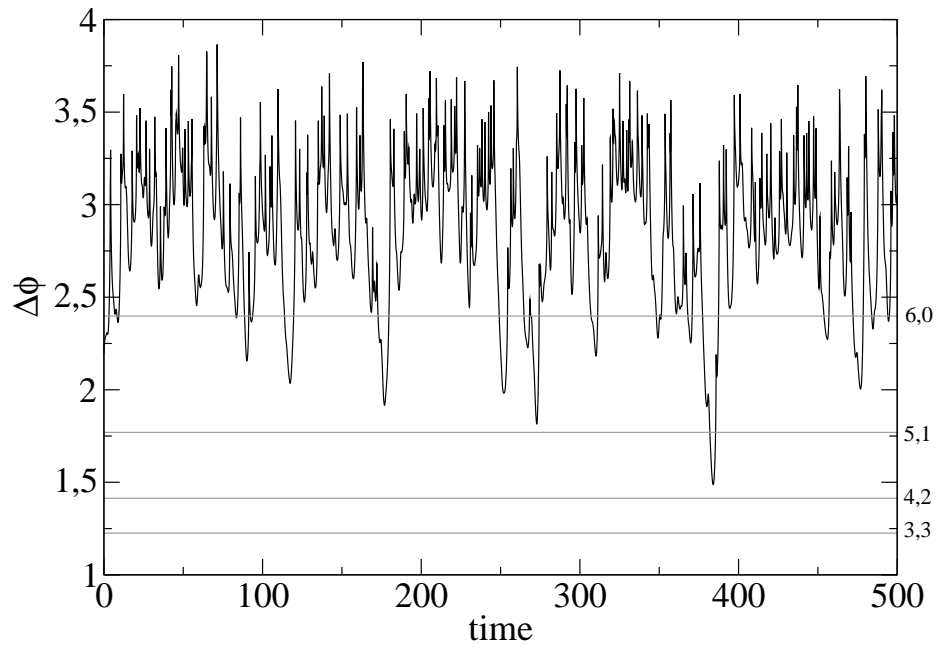


Figure 11: Amplitude versus time with Neumann boundary conditions for  $1/\nu = 11.5$  and  $a = 0.01$

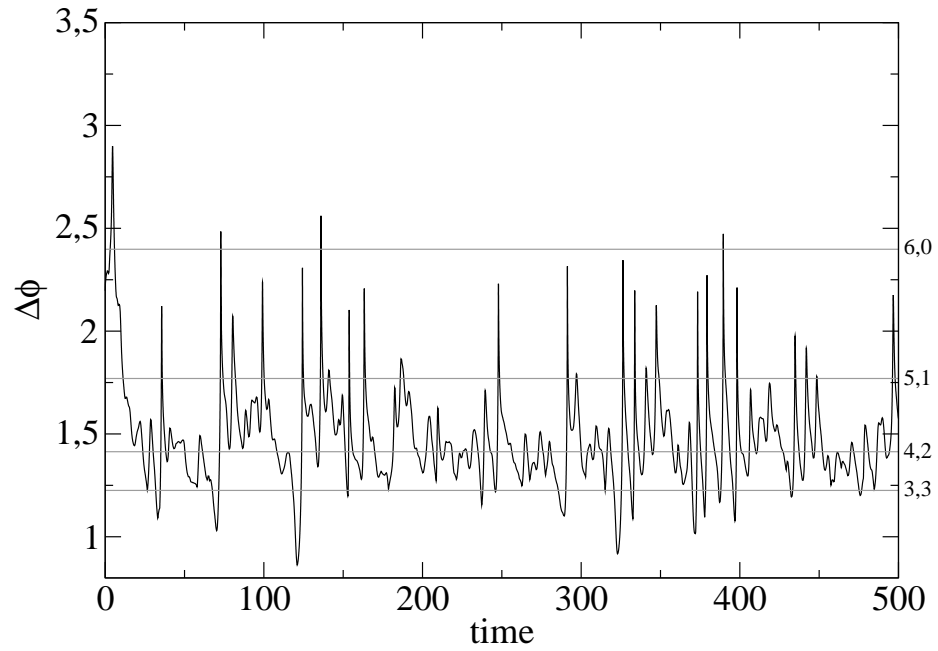


Figure 12: Comparison of the solution at time 410.555 (dashed dotted line) in Figure 11 (Neumann boundary conditions  $1/\nu = 11.5$  and  $a = 0.01$ ) with the stationary (4,2) solution for  $1/\nu = 11.5$  (solid line)

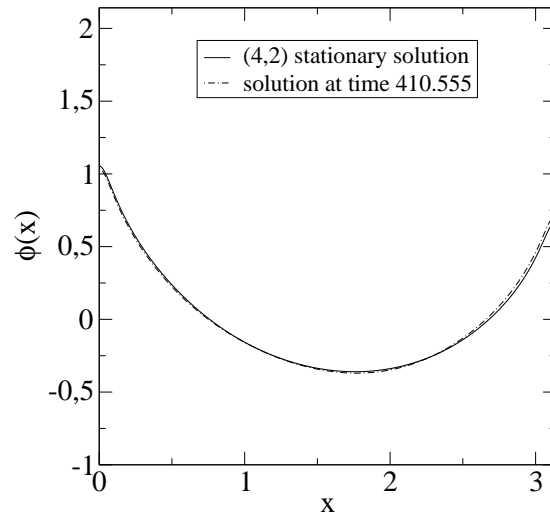


Figure 13: Comparison of the values of  $y_c$  (maximum distance to the real axis of a pole at  $\pi$  to create a new cusp) obtained numerically with a theoretical value obtained by using the continuous approximation of Thual Frisch and Hénon

